Relative performance of two unsaturated soil models using different constitutive variables

Martí Lloret-Cabot, Marti.Lloretcabot@newcastle.edu.au, University of Newcastle, Callaghan, Building EA, NSW 2308, Australia

Simon J. Wheeler, Simon.Wheeler@glasgow.ac.uk, University of Glasgow, School of Engineering, Rankine Building, Glasgow G12 8LT, UK

Jubert A. Pineda, Jubert.pineda@newcastle.edu.au, University of Newcastle, Callaghan, Building EA, NSW 2308, Australia

Daichao Sheng, Daichao.sheng@newcastle.edu.au, University of Newcastle, Callaghan, Building EA, NSW 2308, Australia

Antonio Gens, Antonio.Gens@upc.edu, Universitat Politècnica de Catalunya, C. Jordi Girona 1-3, Mòdul D2, 08034,Barcelona, Spain

Correspondence to: Martí Lloret Cabot, University of Newcastle, Callaghan, NSW 2308, Australia, Phone: +61 2 4921 5660/ +61 2 4921 8832, Marti.Lloretcabot@newcastle.edu.au

Abstract:

Mechanical and water retention behaviour of unsaturated soils is investigated in the context of two well established coupled constitutive models, each of which is formulated in terms of a different set of stress state variables or constitutive variables. Incremental relationships describing volume change and variation of degree of saturation are derived for each model. These incremental relationships are used to simulate a set of experimental tests on compacted Speswhite kaolin previously reported in the literature. Six individual tests, involving isotropic compression and various forms of shearing, are analysed in the context of the incremental forms developed and model predictions are then compared against experimental results. The results show that, although each constitutive model uses a different set of constitutive variables and a different scheme for coupling the mechanical and water retention behaviour, the two sets of model predictions are similar and both sets provide a reasonable match to the experimental results, suggesting that both models are able to capture the relevant features of unsaturated soil behaviour despite expressing the constitutive laws in different ways.

Keywords: constitutive modelling; unsaturated soils; mechanical behaviour; water retention; suction

Introduction

Correct consideration of mechanical and water retention behaviour, together with their coupling, is of fundamental importance in unsaturated soil mechanics. This is generally achieved with the formulation of constitutive models that attempt to both describe the basic physical mechanisms involved and to capture observed patterns of behaviour. The formulation of a constitutive model is therefore typically based on a combination of a theoretical formulation and experimental observations, with the latter also employed in the validation process by comparing model results with those measured in the laboratory.

A large number of constitutive models for unsaturated soils have been proposed since the first elasto-plastic mechanical model in 1990, the well-known Barcelona Basic Model or BBM (Alonso, Gens and Josa, 1990). Summaries of constitutive models for unsaturated soils are available in various review articles (Gens, 1996; Wheeler and Karube, 1996; Jommi, 2000; Gens et al., 2006; Sheng et al. 2008b; Gens, 2010; Sheng, 2011).

Although it is generally accepted that at least two constitutive variables (Jommi, 2000) are required to correctly represent the main features of unsaturated soil behaviour, there is some controversy concerning their choice. In many models, it is possible to distinguish (Gens, 2010) a first constitutive variable (FCV) intended to account for the overall stress state of the soil and a second constitutive variable (SCV) associated with the effects of suction variations. In most cases they can be expressed as:

$$\text{FCV:} \quad \sigma_{ij} - u_a \delta_{ij} + \mu_1 \left(s, S_r \right) \delta_{ij} \tag{1}$$

$$\text{SCV:} \quad \mu_2 \left(s, S_r \right) \tag{2}$$

where σ_{ij} is the total stress tensor, u_a is the pore air pressure, s is the matric suction and δ_{ij} is the Kronecker's delta. μ_1 and μ_2 are general functions that may depend on suction, degree of saturation S_r or both. It is useful to classify the constitutive laws according to the choice of the FCV (Gens, 1996):

- Class I models adopt a FCV with $\mu_1 = 0$.
- Class II models adopt a FCV with $\mu_1(s)$.
- Class III models adopt a FCV with $\mu_1(s, S_r)$.

A similar classification, with different nomenclature, has been presented and discussed in Nuth & Laloui (2008). Advantages and disadvantages of each choice are also discussed in Gens (2010).

It is worth noting that Houlsby (1997) demonstrated that there are several appropriate sets of work-conjugate stress and strain variables for unsaturated soils. He showed (under reasonably general conditions) that the increment of work input dW per unit volume of unsaturated soil can be written as:

$$dW = \left[\sigma_{ij} - \left(S_r u_w + \left(1 - S_r\right) u_a \right) \delta_{ij} \right] d\varepsilon_{ij} - \left(u_a - u_w\right) n dS_r = \sigma_{ij}^{*} d\varepsilon_{ij} - s^{*} dS_r \quad (3)$$

where σ_{ij}^{*} will be referred to as the Bishop's stress tensor, $d\varepsilon_{ij}$ is the strain increment tensor, n is the porosity and s^{*} will be referred to as the modified suction. Equation 3 shows that if Bishop's stress tensor and modified suction are employed as stress state variables to describe unsaturated soil behaviour, the appropriate pair of *work-conjugate* strain increment variables are increments of strains and decrements of the degree of saturation respectively. As pointed out in Houlsby (1997) Equation 3 can be re-arranged to provide other possible choices of stress and strain variables.

Houlsby's Equation 3 also indicates the necessary presence of two basic inter-related constituents in the description of unsaturated soil behaviour: a mechanical part (represented by stress and strain terms) and a retention part (represented by suction and degree of saturation). The approach adopted to describe this mechanical-retention coupling is a key component of any unsaturated soil constitutive model and is also a source of important differences between different formulations. It should be noted that adopting Bishop's stress as the FCV already provides a first degree of mechanical-retention coupling but it is generally insufficient to encompass fully the observed unsaturated soil behaviour.

This paper aims to explore some of these issues by reference to two well-established coupled constitutive models. The first model, hereafter referred to as the SFG model, combines the formulation proposed in Sheng et al. (2008a) with the coupled relationships between mechanical and water retention behaviour proposed by Sheng & Zhou (2011). The constitutive model proposed by Wheeler et al. (2003), including the extended form to general stress states (Lloret-Cabot et al., 2013), is the second model considered. The two models provide a very convenient platform for this discussion because they share a common basic framework (hardening plasticity) but they also exhibit important differences. Thus, the SFG model is formulated in terms of conventional stress variables (net stress tensor and matric suction) and belongs to Class I. In contrast, the Wheeler et al. (2003) model is formulated using Bishop's stress tensor and modified suction as constitutive variables and belongs, therefore, to Class III. As described below, the two models also employ different strategies regarding mechanical-retention coupling.

For each model, a pair of incremental relationships describing volume change and variation of degree of saturation are derived to investigate how the coupled constitutive models account for the mechanical behaviour, the water retention behaviour and their coupling. These incremental relationships have proved to be a very useful tool (particularly when the constitutive laws are relatively complex) to check and explore further the capabilities of a constitutive model. This is of particular interest when describing coupled behaviour, as demonstrated, although in the context of a different constitutive framework, in Mašin (2010).

Results from a substantial experimental program carried out by Sivakumar (1993) on specimens of compacted Speswhite kaolin are used to evaluate the performance of the proposed incremental relationships. Model predictions are compared against experimental results in terms of the variations of

void ratio e and degree of saturation S_r. The contribution that each individual term of these mathematical relationships has on the predicted changes of e and S_r is investigated for various stress paths, involving isotropic (wetting and loading) and shearing stages.

The constitutive models

The formulations of the SFG and Wheeler et al. (2003) models have been previously described in Sheng et al (2008a) and Wheeler et al. (2003), respectively. For the sake of simplicity, only the main features of each model are summarised here (see Table 1). The derivations of the incremental relationships for both mechanical and water retention behaviour are presented in the following sections.

The SFG model is formulated in terms of the mean net stress $\overline{p}$, the deviator stress q and the matric suction s, whereas the Wheeler et al. (2003) model is expressed in terms of the mean Bishop's stress p^*, the deviator stress q and the modified suction s^*.

Both models are formulated in the triaxial stress space and they both adopt the Modified Cam Clay model (Roscoe and Burland, 1968) as the underlying model for saturated conditions. Three yield surfaces are considered in both models as follows (see Table 1): a Loading Collapse (LC) yield surface to describe mechanical behaviour; and Suction Increase (SI) and Suction Decrease (SD) yield surfaces for water retention behaviour (Figure 1). Yielding on the LC yield surface causes plastic volumetric and plastic deviatoric strains (mechanical behaviour) whereas yielding on the SI or SD yield surfaces causes irreversible changes of degree of saturation (retention behaviour).

The specific forms of the yield surfaces to account for reversible and irreversible behaviour are, however, significantly different in each of the models (see Table 1). In particular, when plotted in the s: $\overline{p}$ plane, for isotropic stress states, the forms of the LC, SI and SD yield curves adopted in the SFG model are illustrated in Figure 1a, with their respective extended forms to triaxial stress states shown in Figure 1c. Similarly, the adopted yield surfaces in the Wheeler et al. (2003) model are presented in Figures 1b and 1d when plotted, respectively, in the s^*:p^* plane (isotropic stress states) and in the q:p^*:s^* space (triaxial stress states). Note that the use of the new constitutive variables p^* and s^* in the formulation of the Wheeler et al. (2003) model results in very simple shapes of the yield curves for isotropic stress states (Figure 1b) as some of the complexity associated with coupled behaviour is partly accounted for by the specific form of the constitutive variables p^* and s^* (Equations 12 and 14 in Table 1). Conversely, the SFG model is formulated in terms of simpler constitutive variables $\overline{p}$ and s (Equations 4 and 6) resulting in more complex shapes of the yield curves (Figure 1a). In addition, the use of different constitutive variables is also reflected in how each model accounts for the variation of the apparent tensile yield stress with suction (see Figure 1).

A particular fingerprint of each model is the way of accounting for the coupling between mechanical and water retention behaviour. The original formulation of the SFG model (Sheng et al. 2008a) does not explicitly account for the effects of degree of saturation on volume change behaviour. The

influence of water retention on mechanical behaviour is essentially considered through the effects of suction on volume change. The version of the SFG model presented here, which combines its original formulation with the coupled relationships proposed by Sheng & Zhou (2011), considers the effects of degree of saturation on mechanical behaviour through a relationship between S_r, s and e (void ratio). In other words, for a given value of suction, the effects of degree of saturation on shear strength are reflected through void ratio. On the other hand, the influence of mechanical behaviour on water retention is considered in the SFG model by including the effects of void ratio variations (through total volumetric strains) on degree of saturation (Sheng and Zhou, 2011).

The Wheeler et al. (2003) model, in contrast, accounts for the coupled behaviour in two complementary ways. Firstly by the use of coupled constitutive variables, as Bishop's stresses involve suction and degree of saturation in their definition and the definition of modified suction includes porosity (see Equations 12 and 14). Secondly, and perhaps more importantly, the mechanical-retention coupling is represented by coupled movements of the three yield surfaces.

Using the Bishop's stress as a stress state variable of the model means that for a given stress state defined by $\overline{p}$ and s, the critical state shear strength for a soil sheared at a constant mean net stress and a constant suction, may vary depending on the initial value of degree of saturation (Lloret et al., 2010 and Lloret-Cabot et al., 2013). Some experimental evidence reflecting the effect of degree of saturation (in addition to void ratio) on mechanical behaviour of unsaturated soils is provided in Sun et al. (2010).

In the Wheeler et al. (2003) model, yielding on the SI yield surface (or the SD yield surface) causes irreversible changes of degree of saturation, which produces coupled outward (or inward) movements of the LC yield surface. This coupled movement of the LC yield surface is how the model describes the influence of water retention on the mechanical behaviour and is a consequence of increasing (or decreasing) the stabilising effect of meniscus water bridges around inter-particle contacts (or inter-aggregate contacts) as additional meniscus water bridges form (or disappear) when yielding on the SI (or SD) yield surface.

The influence of mechanical behaviour on water retention is described by a second coupled movement. Yielding on the LC yield surface causes plastic volumetric strains and produces coupled upward movements of the SI and SD yield surfaces. These coupled movements of the SI and SD yield surfaces describe the influence (on the water retention) of reducing the dimensions of the voids and of the connecting passageways between voids when yielding on the LC yield surface (Wheeler et al., 2003).

Mechanical behavior

To investigate how each constitutive model describes volume changes it is useful to express increments of volumetric strains $d\varepsilon_v$ (or, equivalently, increments of void ratio de or specific volume dv) in terms of the increments of the constitutive variables that contribute to volume variations.

For the SFG model, a suitable form to express $d\varepsilon_v$ is in terms of the increments of mean net stress $d\overline{p}$, deviator stress dq and matric suction ds:

$$d\varepsilon_v^{Total} = A_{SFG}^j d\overline{p} + B_{SFG}^j dq + C_{SFG}^j ds \qquad \text{where } j = \text{elastic, LC, SD/SI} \qquad (18)$$

where the specific forms of the functions $A_{SFG}{}^j$, $B_{SFG}{}^j$ and $C_{SFG}{}^j$ depend on the elastic/plastic mechanism active (see Appendix A).

For the Wheeler et al. (2003) model, it is convenient to express the increments of volumetric strains, in terms of the increments of the mean Bishop's stress dp^* and deviator stress dq and the plastic decrement of degree of saturation $-dS_r^p$:

$$d\varepsilon_v^{Total} = A^j dp^* + B^j dq + C^j \left(-dS_r^p\right) \qquad \text{where } j = \text{elastic, LC, SD/SI or LC + SD/SI} \qquad (19)$$

where the specific forms of the functions A, B and C depend on the elastic/plastic mechanism active (see Appendix B).

Equations 18 and 19 express the total increment of volumetric strain as a contribution of three terms. The first term accounts for the isotropic part of the stress state ($d\overline{p}$ and dp^* for the respective model) whereas the second accounts for the deviatoric part (dq). The last term represents the coupling of the water retention on mechanical behaviour (involving ds and $-dS_r^p$ for the respective model). Note, however, that function C in Equation 19 only contributes to $d\varepsilon_v$ for simultaneous yielding on the LC and SD/SI surfaces (see Appendix B). During other types of soil behaviour (i.e. j = elastic, yielding on the LC alone or yielding on the SD/SI alone) $-dS_r^p = 0$ or $C = 0$.

Water retention behavior

Similar expressions can be derived for the increment of degree of saturation dS_r. For the SFG model, a suitable form to express dS_r is in terms of ds and $d\varepsilon_v$:

$$dS_r^{Total} = D_{SFG}^j ds + E_{SFG}^j d\varepsilon_v \qquad \text{where } j = \text{elastic, LC, SD/SI} \qquad (20)$$

where the specific forms of the functions $D_{SFG}{}^j$ and $E_{SFG}{}^j$ depend on the elastic/plastic mechanism active (see Appendix A). Note that combining Equation 20 with Equation 18, the increment of degree of saturation can be also expressed in terms of $d\overline{p}$, dq and ds (see Sheng & Zhou, 2011).

For the Wheeler et al. (2003) model, it is more convenient to express dS_r in terms of the increments of the modified suction ds^* and plastic volumetric strain $d\varepsilon_v^p$:

$$dS_r^{Total} = D^j ds^* + E^j d\varepsilon_v^p \qquad \text{where } j = \text{elastic, LC, SD/SI or LC + SD/SI} \qquad (21)$$

where the specific forms of the functions D and E depend on the elastic/plastic mechanism active (see Appendix B).

Equations 20 and 21 provide general expressions for total changes of degree of saturation as a separate contribution of two terms. The first term in each equation accounts for the contribution of suction (or modified suction in the Wheeler et al., 2003 model). In the SFG formulation the first term alone is equivalent to the classical form of the water retention behaviour when the influence of the mechanical behaviour is neglected as proposed, for example, in van Genuchten (1980) or Fredlund and Xing (1994) (Sheng and Zhou, 2011). The second term in Equation 20 describes how the SFG model accounts for the coupling of the mechanical behaviour on the water retention (through total volumetric strains $d\varepsilon_v$). In contrast, in the Wheeler et al. (2003) model, both terms in Equation 21 account for coupled behaviour. Note, however, that function E in Equation 21 only contributes to dS_r for simultaneous yielding on LC and SD/SI (see Appendix B). During other types of soil behaviour (i.e. j = elastic, yielding on the LC alone or yielding on the SD/SI alone) $d\varepsilon_v^p = 0$ or $E = 0$.

Experimental results

Six experimental tests comprising isotropic and triaxial compression stress paths at constant suction have been used to investigate the capabilities of each model (Figure 2). The tests selected were carried out by Sivakumar (1993) on statically compacted samples of Speswhite kaolin using a suction controlled triaxial cell. Triaxial specimens were compacted at a moisture content of 25% (4% less the optimum from the Standard Proctor test) and a dry density of 1.20Mg/m^3, which corresponded to a vertical compaction stress of 400 kPa and an initial (as-compacted) suction of approximately 700 kPa (additional details are given in Sivakumar, 1993 and Wheeler & Sivakumar, 1995). Each of the tests involved three stages: (i) wetting and equalization to target suction (s = 300 kPa for tests 1R, 2R and 5V; s = 100 kPa for tests 3P, 4P and 6V) (ii) isotropic compression to virgin state under constant suction, and (iii) shearing at constant suction to critical state under three types of conditions. Type R tests involved shearing at constant radial net stress. In Type P tests, the mean net stress remained constant during shearing and in Type V tests shearing was applied at constant volume. A control system was used in Type V tests to increase u_a and u_w by equal amounts (maintaining constant suction) in such a way as to keep the sample volume constant during shearing while maintaining the cell pressure constant (Wheeler and Sivakumar, 1995). Table 2 summarises the stress paths followed in each test.

Tests 1R, 2R and 5V were subjected initially to wetting at constant mean net stress of 50 kPa to reach the value of suction of s = 300 kPa (point A in Figure 2). This state has been used as a common starting point for all the simulations described below. The experimental data showed a significant increase in degree of saturation during the wetting from the as-compacted suction to s = 300 kPa, indicating that A was on the SD yield surface. No collapse compression behaviour was observed during this initial equalization (Sivakumar, 1993) which indicates that the LC yield surface was not reached and, hence, the initial state A was inside the LC yield surface.

Numerical simulations and analysis of soil behavior

The values of constitutive parameters used in the simulations for each of the models are summarised in Table 3. The parameters used in the simulations of the SFG model are: λ_{vp} and κ_{vp} to represent, respectively, the elasto-plastic and elastic volumetric strains caused by mean net stress changes; λ_{ws} and κ_{ws} are, respectively, the gradients of the main wetting and scanning curves in the S_r:ln$s$ plane; m is a soil parameter to describe the influence of void ratio on the water retention; M is the slope of the critical state line in the q: $\bar{p}$ plane; and υ is Poisson's ratio (further details on the SFG model parameters and their determination can be found in Sheng et al., 2008a; Zhou & Sheng, 2009 and Sheng & Zhou, 2011). The parameter values used in the simulations of the Wheeler et al. (2003) model are: λ and κ to represent the gradient of a saturated normal compression line and swelling line respectively in the e:lnp^* plane (which becomes the conventional e:lnp' plane for saturated conditions, where p' is the mean effective stress); λ_s and κ_s are the respective gradients of the main wetting/drying and scanning curves in the S_r:lns^* plane; k_1 and k_2 are the two coupling parameters describing the influences between mechanical and water retention behaviour and $\bar{M}$ is the slope of the critical state line in the q:p^* plane (for further details see Wheeler et al., 2003; Lloret, 2011 and Lloret-Cabot et al., 2013).

The initial state for model calculations is presented in Table 4 and corresponds to point A in Figure 2, i.e. the soil state after equalization at s = 300 kPa and a mean net stress of 50 kPa. As illustrated later, the initial value of the hardening parameter defining the initial position of the LC yield surface can be estimated from the sharp discontinuity observed when plotting the experimental results in the e:ln $\bar{p}$ plane (for the SFG model) or the e:lnp^* plane (for the Wheeler et al. 2003 model). The initial values of e and S_r employed are those corresponding to the average of the tests at s = 300 kPa (i.e. 1R, 2R and 5V). From this initial state (Table 4) a wetting path at a constant mean net stress of 50 kPa from s = 300 kPa to s = 100 kPa was modelled for the tests performed at s = 100 kPa (i.e. 3P, 4P and 6V) (see path AB in Figure 2).

The stress paths are illustrated in Figure 2 (see also Table 2). Figure 2a presents the stress paths for the SFG model in the conventional q: $\bar{p}$:s space whereas Figure 2b shows the stress paths for the Wheeler et al. (2003) model in q:p^*:s^* space. A detailed discussion of the performance of the models in simulating the stress paths plotted in Figure 2 is given in the following sub-sections below. In all the following figures, the experimental results are indicated by symbols joined by fine lines, whereas the model simulations are indicated by heavier lines.

Type R and P tests

As indicated above, Type R tests involved shearing under constant radial net stress whereas shearing of Type P tests was performed under constant mean net stress. Figures 3-8 show the variation of degree of saturation S_r and void ratio e for Type R tests (1R and 2R) and Type P tests (3P and 4P), plotted against

mean net stress $\overline{p}$ (Figures 3ac, 4ac, 5ac and 6ac), mean Bishop's stress (Figures 3bd, 4bd, 5bd and 6bd) and deviator stress (Figures 7 and 8). Figures 3, 5 and 7 show the performance of the SFG model, whereas Figures 4, 6 and 8 show the simulations of the Wheeler et al. (2003) model.

As discussed earlier, point A in Figures 3-6, which is on the SD yield surface but inside the LC yield surface, corresponds to the common starting point of all simulations, with AB representing simulation of initial wetting from s = 300 kPa to s = 100 kPa for those tests performed at s = 100 kPa. Experimental results and model simulations in Figure 3-6 cover both isotropic loading stages and subsequent shearing stages. Point X in each simulation indicates the end of the isotropic loading stage and the start of the shearing stage, whereas point C indicates the final critical state at the end of shearing. Subscripts on X or C indicate the individual test number.

Isotropic stress stages

During the initial part of the isotropic loading stages at constant suction, the SFG model predicts a reduction of e which is the result of elastic volumetric strain caused by the increase in $\overline{p}$ (Figures 3cd and 5cd). Note that only the term involving $\mathrm{d}\overline{p}$ (see Equation 18) contributes to the predicted volumetric strain variations (as $\mathrm{d}s$ = 0 and $\mathrm{d}q$ = 0 throughout the isotropic loadings). The elastic volumetric strain during the early part of the isotropic loading causes a very small increase of S_r (hardly noticeable in the SFG simulations in Figures 3ab and 5ab) which is described by the second term of Equation 20 accounting for the influence of volumetric strain on S_r. In contrast, the simulations of the Wheeler et al. (2003) model involve yielding on the SD yield surface during the initial part of the isotropic loadings, because of the reduction of s^* caused by a reduction of porosity (which is, in turn, the result of elastic volumetric strain caused by the increase in p^*) (see Figures 4cd and 6cd). The decrease of s^* during this early part of the loading stage is very small and, as a consequence, the predicted increases of S_r (which include both elastic and plastic components) are also very small (Figures 4ab and 6ab).

At a point during each isotropic loading stage, the stress paths in both model simulations reach the LC yield surface. These yield points are indicated by Y in Figures 3-6. Yielding on the LC yield surface results in predictions of large reductions of e (plastic deformation) from the yield point onwards (see Figures 3-6). The large decrease of e predicted by the SFG model in this later part of the isotropic loading stages is described by Equation 18, where $\mathrm{d}\overline{p}$ is the only non-zero term (Figures 3cd and 5cd). Additionally, this reduction of e predicted by the SFG model causes a substantial increase of S_r (Figures 3ab and 5ab) as a consequence of the coupling term defining how the void ratio influences the water retention behaviour (second term in Equation 20). In contrast, the large increase of S_r predicted by the Wheeler et al. (2003) model from the point where the LC yield surface is reached arises from the combination of several components. From Y onwards the model predicts simultaneous yielding on the SD and LC surfaces. Yielding on the LC yield surface results in predictions of large plastic decreases of void ratio e after the yield point (Figures 4cd and 6cd). This yielding on the LC yield surface and the resulting plastic volumetric strain (Equation 19 with j = LC + SD) also produces both a significant

reduction of s^*, as the porosity reduces, and coupled upward movement of the SD yield surface. Together these result in predictions of significant yielding on the SD yield surface, and hence large plastic increases of S_r after the yield point (Figures 4ab and 6ab).

Note that Figures 5 and 6 include the modelling of initial wetting from s = 300 kPa to s = 100 kPa for Tests 3P and 4P. The modelling of this initial wetting AB is indicated in the figures by a heavy dashed line (Figures 5 and 6). Both models provide a remarkably similar response, predicting a small amount of swelling and a large increase of degree of saturation as a consequence of yielding on the SD yield surface. Note that the increase of void ratio during this initial wetting is a result of elastic volumetric strain caused by a decrease in s for the SFG model (third term in Equation 18) and by a decrease in p^* for the Wheeler et al. (2003) model (Equation 19).

Inspection of Figures 3-6 shows that, during the isotropic stress paths, both models provide a good match to the experimental results for both void ratio and degree of saturation. A sharp discontinuity of gradient is observed in the model simulations at the yield point Y where the LC yield surface is reached (Figures 3-6). This is due to the use (in both models) of classical elasto-plasticity for the modelling framework which could be enhanced by incorporating the concepts of sub-loading (Nakai and Hinoko, 2004) or generalised plasticity theories (Sánchez et al., 2005).

Shearing stages

The transition from isotropic loading to shearing stages is smoother in Type R shear tests (where the radial net stress remains constant) than in Type P shear tests (where the mean net stress is maintained constant), because the change of stress path direction is more dramatic in the latter case. This is true for both experimental results and model predictions. Both models predict large decreases of e and large increases of S_r throughout the shearing stages of these tests (Figures 3-8).

Comparison of the model predictions and experimental results in these figures leads to similar conclusions as the previous discussion around the isotropic loading stages of Types R and P tests. In particular, the significant reduction of e predicted by the SFG model (see Figures 3cd, 5cd and 7b) is governed by Equation 18 (with j = LC) now accounting also for the role of deviator stress changes (second term in Equation 18). Note that for Type P shear tests this second term is the only contribution to volumetric strain variations (as $\mathrm{d}\overline{p} = 0$). The reduction of e is coupled with the degree of saturation variations (second term in Equation 20) causing the predicted large increase of S_r throughout the shearing stages of Types R and P (see Figures 3ab, 5ab and 7a).

The Wheeler et al. (2003) model predicts not only yielding on the LC yield surface during the shearing stages of Types R and P tests, but also yielding on the SD yield surface, which produce respectively large plastic volumetric strains (and, hence, predictions of large reductions of e) and large plastic increases of S_r (see Figures 4, 6 and 8).

The SFG model predictions of the variation of void ratio during Types R and P shearing are a slightly

more accurate match to the experimental variations of e than the corresponding predictions from the Wheeler et al. (2003) model. Also the predicted SFG critical state values for e show a reasonably good match to the experimental data whereas the results from the Wheeler et al. (2003) model are in general somewhat over-predicted. On the other hand, the Wheeler et al. (2003) model predictions of the variation of degree of saturation during Types R and P shear tests are slightly more accurate than the variations of S_r predicted by the SFG model. The predicted critical state values of S_r are also a reasonable match to the experimental data when using the Wheeler et al. (2003) model. Slightly less successful are the predicted critical state values of S_r by the SFG model. Both models provide satisfactory predictions of the final critical state values of deviator stress q (and hence the shear strength) in these tests (Figures 7 and 8), as a consequence of achieving reasonable predictions of the stress paths (see below).

Type V tests

Probably a sterner check on the performance of the two constitutive models is provided by Type V tests in which non-conventional constant volume shearing was applied. Figures 9-12 show the variation of degree of saturation S_r and void ratio e for Type V shear tests (see Table 2). The results are plotted against mean net stress (Figures 9ac and 10ac); mean Bishop's stress (Figures 9bd and 10bd) and deviator stress (Figures 11 and 12). Figures 9 and 11 show the performance of the SFG model whereas simulations of the Wheeler et al. (2003) model are shown in Figures 10 and 12. Again, the starting point of all simulations corresponds to A at s = 300 kPa.

Comparison between model predictions and experimental results for the isotropic loading stages of Type V tests leads to equivalent conclusions to those given for Type R and P tests during their isotropic loading stages.

During shearing of Type V the mean net stress $\overline{p}$ (and as a consequence also the mean Bishop's stress p^*) is decreased in order to maintain the volume constant. The predicted reductions of $\overline{p}$ (and p^*) required to reach the critical state are over-predicted in both models and, hence, the stress paths are not accurately predicted (see below). As a consequence, the critical state value of q (and hence the shear strength) is generally under-predicted in both cases. These discrepancies between simulations and experimental data can be attributed to the choice of an elliptical cross-section for the LC yield surface together with the adoption of associated plasticity.

With the SFG model, S_r (as well as e) is predicted to remain constant throughout the shearing process (Figure 11). Within the model, the decrease of $\overline{p}$ produces sufficient negative volumetric strain to cancel out the positive component of volumetric strain produced by the increase of q (Equation 18) as a consequence of yielding on the LC surface. As a result of maintaining the volume (and suction) constant during shearing, the SFG model predicts that S_r also remains constant (see Equation 20), although the experimental data shows a modest increase of S_r during these tests.

The Wheeler et al. (2003) model predicts simultaneous yielding on LC and SD surfaces throughout the shearing stages. During shearing of Type V the model predicts small amounts of yielding on the LC yield surface, sufficient to produce enough positive plastic volumetric strain to offset the negative elastic volumetric strain predicted from the decrease of p^*. The model predicts only a very small increase of S_r during the shearing process (Figure 12). No elastic changes of S_r are predicted by the model during these tests because the modified suction remains constant (because both suction and porosity are constant). There are, however, small plastic increases of S_r predicted by the model, because simultaneous yielding on LC and SD yield surfaces is occurring during shearing. The reason that the model predicts plastic increases of S_r during these tests is essentially because, within the Wheeler et al. (2003) model, the influence of changing void ratio on the water retention behaviour is assumed to be caused only by plastic volumetric strains (see the final term in Equation 21). Elastic volumetric strains are assumed to have no influence on the shift of the retention curves when plotted in the S_r: lns^* plane. In these Type V tests, plastic volumetric strains are occurring (even though there are no total volumetric strains), and these plastic volumetric strains have an impact on the predicted water retention behaviour, with the effect that changes of S_r are predicted (albeit very small) during shearing.

Predicted and experimental stress paths

Figure 13 shows the simulations of the stress paths by the two models plotted against mean net stress (Figures 13a and 13c) and against mean Bishop's stress (Figures 13b and 13d). Parts a and b of Figure 13 show the predicted stress paths for the SFG model whereas parts c and d show the counterparts for the Wheeler et al. (2003) model. Also shown are the corresponding experimental stress paths. The experimental stress paths are reasonably well predicted for Types R and P constant suction shear tests, where the radial net stress and the mean net stress respectively remained constant. Note that shearing stress paths for Type R tests rise at a gradient of 3 when plotted in the q: $\overline{p}$ plane, and shearing stress paths for Type P are vertical in the q: $\overline{p}$ plane (Figure 13a and 13c). In contrast, Figures 13b and 13d show that the stress paths for Type R shear tests do not rise at a gradient of 3 when plotted against mean Bishop's stress, due to the influence of S_r on p^* (this is true for both experimental results and model predictions). Similarly, the stress paths for Type P shear tests are not vertical in the q:p^* plane, because the variation of S_r during shearing means that p^* does not remain constant (again, this is true for both experimental results and model predictions). As described above, less accurate predictions are obtained for the shearing stress paths of Type V shear tests, where the decrease of mean net stress to maintain the specific volume constant during shearing is in general over-predicted.

Conclusions

Coupled mechanical-retention behaviour of unsaturated soils has been studied in the context of two different constitutive models that include, in their formulation, mechanical and water retention responses and the coupling between them. The two models are expressed in terms of two different sets of constitutive variables and, according to the classification proposed in Gens (2010), they belong to

different classes of model. For each model, incremental relationships describing variations of void ratio e and degree of saturation S_r have been derived in terms of the corresponding constitutive variables and these incremental relationships have subsequently been used to compare model predictions with experimental data from the suction controlled triaxial tests of Sivakumar (1993).

The main differences between the two model formulations used here are in terms of the constitutive variables used, the specific forms of the yield surfaces and how the model accounts for the coupling between mechanical and retention behaviour. For example, under isotropic stress conditions, each model uses a different approach to describe the influence of mechanical behaviour (changes of void ratio) on the water retention behaviour, although their predictions are reasonably similar. The SFG formulation includes a specific mathematical form for the variation of degree of saturation that directly accounts for the influence of void ratio (through total volumetric strains), whereas the Wheeler et al. (2003) model assumes that the influence of mechanical behaviour on water retention is essentially caused only by plastic volumetric strains.

Simulations performed with each model are interpreted in the context of the incremental relationships for S_r and e. Both models are capable of reproducing the main features of unsaturated soil behaviour observed in the experimental tests. In addition, the simulations show that the two models produce not only qualitatively similar predictions but also quantitatively similar results that show good matches with the experimental data. This suggests that, although the two models are formulated very differently, both formulations are capable of adequately capturing the mechanical and retention behaviour of unsaturated soils. This is consistent with the results of a benchmarking exercise reported in D'Onza et al. (2011).

Although the predictions during shearing are qualitatively similar for both models, small quantitative discrepancies are observed. In general, during the shearing stages of the tests analysed, the SFG model appears to be more successful in predicting the mechanical behaviour (variation of void ratio) whereas the Wheeler et al. (2003) model appears to provide better predictions for the water retention response (variation of degree of saturation). For example, the predicted values of e at critical state from the SFG model are reasonably accurate in most of the simulations whereas in the Wheeler et al. (2003) model they are typically over-predicted. On the other hand, the Wheeler et al. (2003) model predicted values of S_r at critical state more accurately than the SFG model.

During shearing at constant volume (Type V tests) both models over-predict the reduction of mean net stress required to maintain the volume constant. As a consequence, the critical state values of deviator stress are under-predicted by both models in these tests. These weaknesses of the models can be attributed to their common assumption of an elliptical yield curve shape combined with an associated flow rule (both inherited from the Modified Cam Clay base model for saturated conditions).

The Wheeler et al. (2003) model predicts increases (although very small) of degree of saturation during constant suction constant volume shearing stages of Type V tests as a consequence of assuming that the influence of changing void ratio on water retention behaviour is caused only by plastic volumetric

strains. Interestingly, the experimental results for all the Type V shear tests of Sivakumar (1993) consistently show a modest increase of S_r during the shearing process, which might be interpreted as qualitative support for the assumption in the model that it is plastic volumetric strain (rather than total volumetric strain) that controls the shift of the water retention curves to higher values of suction when the void ratio reduces.

Moving beyond the relative performance of the two constitutive models, the comparison exercise reported in this paper appears to support the view that a good representation of observed unsaturated soil behaviour can be achieved by models that, though sharing a basic theoretical formulation, adopt quite different assumptions concerning key aspects such as the form of their constitutive variables and the strategy for coupling mechanical and retention behaviour. Of course, this tentative conclusion must be re-apprised for a wider range of experimental results, as the experimental tests of Sivakumar (1993) were limited to compacted samples only and they did not involve any drying stages or cycles of suction variation. Hence, in order to confirm the generality of the conclusions presented here, comparisons between the predictions of the two models and between the model predictions and experimental results, should, in the future, be extended to tests involving a wider range of stress paths and soil types.

Acknowledgements

The work presented here benefited from a New Staff grant (G1301107) from the University of Newcastle and the Research Advisory Group (RAG).

References

Alonso, E.E., Gens, A. & Josa, A. (1990). A constitutive model for partially saturated soils. Géotechnique, **40**, No. 3, 405-430.

Fredlund, D.G., & Xing, A. (1994). Equations for the soil-water characteristic curve. Canadian Geotechnical Journal, **31**, No. 4, 521-532. doi:10.1139/t94-061

Gens, A. (1996). Constitutive modelling: Application to compacted soils. *In* Proceedings of the 1st International Conference on Unsaturated Soils, Paris, France, (E.E. Alonso & P. Delage, eds.). Rotterdam: Balkema 3, 1179-1200.

Gens, A. (2010). Soil-environment interactions in geotechnical engineering. Géotechnique, **60**, No. 1, 3-74 (47th Rankine Lecture).

Gens, A., Sánchez, M. & Sheng, D. (2006). On constitutive modelling of unsaturated soils. Acta Geotechnica, **1**, 137-147.

Houlsby, G.T. (1997). The work input to an unsaturated granular material. Géotechnique, **47**, No. 1, 193-196.

Jommi, C. (2000). Remarks on the constitutive modelling of unsaturated soils. *In* Experimental Evidence and Theoretical Approaches in Unsaturated Soils, Proceedings of International Workshop on Unsaturated Soils, Trento, Italy, (A. Tarantino and C. Mancuso, eds.). Rotterdam: Balkema, 139-153.

Lloret, M. (2011). Numerical modelling of coupled behaviour in unsaturated soils. PhD Thesis, University of Strathclyde and University of Glasgow, UK.

Lloret, M., Sánchez, M., and Wheeler, S. (2010). Generalised elasto-plastic stress-strain and modified suction-degree of saturation relations of a fully coupled model. *In* Proceedings of the 4th Asia-Pacific Conference on Unsaturated Soils, Newcastle, Australia (O. Buzzi, S. Fityus and D. Sheng, eds.). CRC Press-Taylor & Francis Group, 667-672.

Lloret-Cabot, M., Sánchez, M. & Wheeler, S.J. (2013). Formulation of a 3D constitutive model for unsaturated soils incorporating mechanical-water retention couplings. International Journal for Numerical and Analytical Methods in Geomechanics, **37**, 3008-3035. DOI:10.1002/nag.2176.

Mašin, D. (2010). Predicting the dependency of a degree of saturation on void ratio and suction using effective stress principle for unsaturated soils. International Journal for Numerical and Analytical Methods in Geomechanics, **34**, 73-90.

Nakai, T. & Hinoko, M. (2004). A simple model for normally and over consolidated soils with unified material parameters. Soils and Foundations, **44**, No. 2, 53-70.

Nuth, M. & Laloui, L. (2008). Effective Stress Concept in Unsaturated Soils: Clarification and Validation of a Unified Framework, International Journal of Numerical and Analytical Methods in Geomechanics, **32**, No. 7, 771-801.

D'Onza, F., Gallipoli, D., Wheeler, S.J., Casini, F., Vaunat, J., Khalili, N., Laloui, L., Mancuso, C., Mašín, D., Nuth, M., Pereira, J.M. & Vassallo, R. (2011). Benchmark of constitutive models for unsaturated soils. Géotechnique, **61**, No. 4, 283-302.

Roscoe, K.H. & Burland, J.B. (1968). On the generalised stress-strain behavior of wet clay. Engineering Plasticity (eds Heyman J & Leckie FA), Cambridge University Press, Cambridge: 535-609.

Sánchez, M., Gens, A., Guimarães, L. & Olivella, S. (2005). A double structure generalized plasticity model for expansive materials. International Journal for Numerical and Analytical Methods in Geomechanics, **29**, 751-787.

Sheng, D., Fredlund, D.G., & Gens, A. (2008a). A new modelling approach for unsaturated soils using independent stress variables. Canadian Geotechnical Journal, **45**, 511-534.

Sheng, D., Gens, A., Fredlund, D.G. & Sloan S.W. (2008b). Unsaturated soils: From constitutive modelling to numerical algorithms. Computers and Geotechnics, **35**, 810-824.

Sheng, D. (2011). Review of fundamental principles in modelling unsaturated soil behaviour. Computers and Geotechnics, **38**, 757-776.

Sheng, D. & Zhou, A. (2011). Coupling hydraulic with mechanical models for unsaturated Soils. Canadian Geotechnical Journal, **48**, 826-840.

Sivakumar, V. (1993). A critical state framework for unsaturated soil. PhD Thesis, University of Sheffield, UK.

van Genuchten, M.Th. (1980). A closed-form equation for predicting the hydraulic conductivity of unsaturated soils. Soil Science Society of America Journal, **44**, No. 5, 892-898. doi:10.2136/sssaj1980. 03615995004400050002x.

Sun, D.A., Sun, W.J. & Xiang L. (2010). Effect of degree of saturation on mechanical behaviour of unsaturated soils and its elastoplastic simulation. Computers and Geotechnics, **37**, No. 5, 678-688.

Wheeler, S.J. & Karube, D. (1996). Constitutive modelling. *In* Proceedings of the 1st International Conference on Unsaturated Soils, Paris, France, (E.E. Alonso & P. Delage, eds.). Rotterdam: Balkema 3, 1323-1356.

Wheeler, S.J. & Sivakumar, V. (1995). An elasto-plastic critical state framework for unsaturated soil. Geotechnique, **45**, No.1, 35-53.

Wheeler, S.J., Sharma, R.S. & Buisson, M.S.R. (2003). Coupling of hydraulic hysteresis and stress-strain behaviour in unsaturated soils. Géotechnique, **53**, No. 1, 41-54.

Zhou, A. & Sheng, D. (2009). Yield stress, volume change and shear strength behaviour of unsaturated soils: Validation of the SFG model. Canadian Geotechnical Journal, **46**, 1034-1045.

Appendix A

The increments of volumetric strains and degree of saturation for a compacted soil using the SFG model are given by Equations 18 and 20, respectively. The analytical forms of the functions A_{SFG}^{j}, B_{SFG}^{j}, C_{SFG}^{j}, D_{SFG}^{j} and E_{SFG}^{j} presented in this section have been successfully validated for the soil responses of the stress paths investigated. Their specific forms for other stress paths involving different types of soil behaviour (such as yielding on the SI surface) require further investigation as they are not included in the analysis presented in this paper (see, for instance, Sheng and Zhou, 2011).

$$\mathrm{d}\varepsilon_v^{Total} = A_{SFG}^{j}\mathrm{d}\bar{p} + B_{SFG}^{j}\mathrm{d}q + C_{SFG}^{j}\mathrm{d}s \qquad \text{where } j = \text{elastic, LC, SD/SI} \qquad \text{(A1)}$$

$$\mathrm{d}S_r^{Total} = D_{SFG}^{j}\mathrm{d}s + E_{SFG}^{j}\mathrm{d}\varepsilon_v \qquad \text{where } j = \text{elastic, LC, SD/SI} \qquad \text{(A2)}$$

where the specific forms of the functions A_{SFG}^{j}, B_{SFG}^{j}, C_{SFG}^{j}, D_{SFG}^{j} and E_{SFG}^{j} depend on the elastic/plastic mechanism active as follows.

ELASTIC BEHAVIOUR (j = elastic)

$$A_{SFG} = \kappa_{vp}\frac{1}{\bar{p}+s} \qquad \text{(A3)}$$

$$B_{SFG} = 0 \qquad \text{(A4)}$$

$$C_{SFG} = \kappa_{vs}\frac{1}{\bar{p}+s} = \kappa_{vp}\frac{s_{sa}}{s\left(\bar{p}+s\right)} \qquad \text{(A5)}$$

$$D_{SFG} = -\kappa_{ws}\frac{1}{s} \qquad \text{(A6)}$$

$$E_{SFG} = \frac{S_r}{n}\left(1-S_r\right)^{m} \qquad \text{(A7)}$$

where κ_{vp} is a soil constant relating elastic volumetric strains to mean net stress changes; s_{sa} is the saturation value of suction; κ_{ws} is the gradient of a scanning curve in the S_r:ln$s$ plane, m is a soil parameter to account for the influence of void ratio on water retention and n is the porosity.

YIELDING ON THE LC (j = LC) during loading tests at constant suction

$$A_{SFG} = \kappa_{vp}\frac{1}{\bar{p}+s} + \frac{a_{LC}}{H_{LC}}a_{LC} \qquad \text{(A8)}$$

$$B_{SFG} = \frac{a_{LC}}{H_{LC}}b_{LC} \qquad \text{(A9)}$$

$$E_{SFG} = \frac{S_r}{n}\left(1 - S_r\right)^m \tag{A10}$$

where (assuming associated plasticity):

$$H_{LC} = -\frac{\partial f_{LC}}{\partial \overline{p}_{yn}} \frac{\partial \overline{p}_{yn}}{\partial \varepsilon_v^p} \frac{\partial f_{LC}}{\partial \overline{p}} = -\frac{\partial f_{LC}}{\partial \overline{p}_{yn}} \frac{\left(\overline{p}_{yn}(0) + s\right)}{\left(\lambda_{vp} - \kappa_{vp}\right)} \frac{\partial f_{LC}}{\partial \overline{p}} \tag{A11}$$

$$a_{LC} = \frac{\partial f_{LC}}{\partial \overline{p}} \tag{A12}$$

$$b_{LC} = \frac{\partial f_{LC}}{\partial q} \tag{A13}$$

where λ_{vp} is a soil constant relating elasto-plastic volumetric strains to mean net stress changes and $\overline{p}_{yn}(0)$ is the hardening parameter defining the location of the LC yield surface for a compacted soil at zero suction.

YIELDING ON THE SD (j = SD) during wetting tests at constant mean net stress and deviator stress

$$C_{SFG} = \kappa_{vp} \frac{s_{sa}}{s\left(\overline{p} + s\right)} \tag{A14}$$

$$D_{SFG} = -\lambda_{ws} \frac{1}{s} \tag{A15}$$

$$E_{SFG} = \frac{S_r}{n}\left(1 - S_r\right)^m \tag{A16}$$

where λ_{ws} is the gradient of the main wetting curve in the S_r:ln$s$ plane.

Appendix B

The increments of volumetric strains and degree of saturation in the Wheeler et al. (2003) model are given by Equations 19 and 21, respectively:

$$\mathrm{d}\varepsilon_v^{Total} = A^j \mathrm{d}p^* + B^j \mathrm{d}q + C^j \left(-\mathrm{d}S_r^p\right) \qquad \text{where } j = \text{elastic, LC, SD/SI or LC + SD/SI} \tag{B1}$$

$$\mathrm{d}S_r^{Total} = D^j \mathrm{d}s^* + E^j \mathrm{d}\varepsilon_v^p \qquad \text{where } j = \text{elastic, LC, SD/SI or LC + SD/SI} \tag{B2}$$

where the specific forms of the functions A, B, C, D and E depend on the elastic/plastic mechanism active.

ELASTIC BEHAVIOUR (j = elastic)

$$A = \kappa \frac{1}{vp^*} \tag{B3}$$

$$B = 0 \tag{B4}$$

$$D = -\kappa_s \frac{1}{s^*} \tag{B5}$$

where κ is the gradient of a swelling line in the e:lnp^* plane, κ_s is the gradient of a scanning curve in the S_r:lns^* plane and v is the specific volume.

YIELDING ON THE LC ALONE (j = LC)

$$A = \kappa \frac{1}{vp^*} + \frac{\bar{a}_{LC}}{\bar{H}_{LC}} \bar{a}_{LC} \tag{B6}$$

$$B = \frac{\bar{a}_{LC}}{\bar{H}_{LC}} \bar{b}_{LC} \tag{B7}$$

$$D = -\kappa_s \frac{1}{s^*} \tag{B8}$$

$$E = 0 \tag{B9}$$

where:

$$\bar{H}_{LC} = -\frac{\partial f_{LC}}{\partial p_0^*} \frac{\partial p_0^*}{\partial \varepsilon_v^p} \frac{\partial f_{LC}}{\partial p^*} = -\frac{\partial f_{LC}}{\partial p_0^*} \frac{vp_0^*}{(\lambda - \kappa)} \frac{\partial f_{LC}}{\partial p^*} \tag{B10}$$

$$\bar{a}_{LC} = \frac{\partial f_{LC}}{\partial p^*} \tag{B11}$$

$$\bar{b}_{LC} = \frac{\partial f_{LC}}{\partial q} \tag{B12}$$

where λ is the gradient of a saturated normal compression line in the e:lnp^* plane and p_0^* is the hardening parameter defining the location of the LC yield surface.

Note that although $d\varepsilon_v^p$ is not zero when yielding on the LC alone, the second term of Equation B2 does not contribute to the variation of degree of saturation for j = LC (E = 0).

YIELDING ON THE SD/SI ALONE (j = SD or SI)

$$A = \kappa \frac{1}{vp^*} \tag{B13}$$

$$B = C = 0 \tag{B14}$$

$$D = -\lambda_s \frac{1}{s^*} \tag{B15}$$

where λ_s is the gradient of a main wetting/drying curve in the S_r:lns^* plane. Note that although $-\mathrm{d}S_r^p$ is not zero when yielding on the SD/SI alone, the third term of Equation B1 does not contribute to volumetric strains for j = SD or SI (C = 0).

YIELDING ON BOTH THE LC and SD/SI (j = LC + SD or SI)

$$A = \kappa \frac{1}{vp^*} + \frac{\bar{a}_{LC}}{\bar{H}_{LC}} \bar{a}_{LC} \tag{B16}$$

$$B = \frac{\bar{a}_{LC}}{\bar{H}_{LC}} \bar{b}_{LC} \tag{B17}$$

$$C = \frac{\bar{a}_{LC}}{\bar{H}_{LC}} \frac{k_1}{(\lambda_s - \kappa_s)} \frac{\partial f_{LC}}{\partial p_0^*} p_0^* \tag{B18}$$

$$D = -\lambda_s \frac{1}{s^*} \tag{B19}$$

$$E = k_2 \frac{\lambda_s - \kappa_s}{\lambda - \kappa} v \tag{B20}$$

where k_1 and k_2 are two coupling parameters controlling the coupled movements between the yield surfaces (Wheeler et al., 2003).

Table 1. Main features of the constitutive models

<table>
<tr><td></td><td>SFG model (Sheng et al., 2008a)</td><td>Wheeler et al. (2003) model</td></tr>
<tr><td>Stress variables</td><td>$\bar{p} = p - u_a$ (4)
$q = \sigma_1 - \sigma_2$ (5)
$s = u_a - u_w$ (6)</td><td>$p^* = p - S_r u_w - (1 - S_r) u_a = \bar{p} + S_r s$ (12)
$q = \sigma_1 - \sigma_2$ (13)
$s^* = n(u_a - u_w) = ns$ (14)</td></tr>
<tr><td></td><td colspan="2">Notation: p is the mean total stress; σ_1 and σ_2 are the axial and radial total stresses respectively; u_w is the pore water pressure and u_a is the pore air pressure, n is the porosity and S_r is the degree of saturation.</td></tr>
<tr><td>Mechanical yielding</td><td>LC yield surface: (see Figure 1)
$q^2 - M^2 (\bar{p} - \bar{p}_0(s))(\bar{p}_{yn}(s) - \bar{p}) = 0$ (7)</td><td>LC yield surface: (see Figure 1)
$q^2 - \bar{M}^2 p^* (p_0^* - p^*) = 0$ (15)</td></tr>
<tr><td></td><td colspan="2">Notation: M and $\bar{M}$ are soil constants; $\bar{p}_{yn}(s)$ and p_0^* are, respectively, hardening parameters defining the location of the LC surface for the SFG and the Wheeler et al. (2003) models and $\bar{p}_0(s)$ is the apparent tensile yield stress in the SFG model. The variations of the SFG yield stresses $\bar{p}_{yn}(s)$ and $\bar{p}_0(s)$ with suction are given by:
$\bar{p}_{yn}(s) = \begin{cases} \bar{p}_{yn0} - s & s < s_{sa} \\ \dfrac{\bar{p}_{yn0}}{\bar{p}_{y0}} \left(\bar{p}_{y0} + s - s_{sa} - s_{sa} \ln \dfrac{s}{s_{sa}} \right) - s & s \geq s_{sa} \end{cases}$ (8)
$\bar{p}_0(s) = \begin{cases} -s & s < s_{sa} \\ -s_{sa} - s_{sa} \ln \dfrac{s}{s_{sa}} & s \geq s_{sa} \end{cases}$ (9)
where $\bar{p}_{y0}$ is the yield stress at zero suction (for a slurry soil), $\bar{p}_{yn0}$ is the new pre-consolidation pressure at zero suction for a compacted soil and s_{sa} is the saturation value of suction.</td></tr>
<tr><td>Water retention</td><td>SI and SD yield surfaces: (see Figure 1)
$s - s_I = 0$ (10)</td><td>SI and SD yield surfaces: (see Figure 1)
$s^* - s_I^* = 0$ (16)</td></tr>
</table>

yielding	$s_D - s = 0$ (11)	$s_D^* - s^* = 0$ (17)
	Notation: s_I, s_D, s_I^* and s_D^* are hardening parameters defining the location of the SI and SD surfaces, respectively.	

Table 2. Summary of the stress paths

Test type and test number		Suction at equalization stage (kPa)	Mean net stress at the end of isotropic loading (kPa)	Shearing conditions
R	1R	300	100	Constant suction and constant radial net stress
	2R	300	150	
P	3P	100	100	Constant suction and constant mean net stress
	4P	100	200	
V	5V	300	250	Constant suction and constant volume
	6V	100	150	

Table 3. Model parameters values

SFG model	$\lambda_{vp} = 0.16$	$m = 0.05$	$\lambda_{ws} = 0.095$	$M = 0.845$
	$\kappa_{vp} = 0.015$	$p_{y0} = 80$ kPa[1]	$\kappa_{ws} = 0.03$	$\upsilon = 0.3$
Wheeler et al. (2003) model	$\lambda = 0.124$	$k_1 = 0.662$	$\lambda_s = 0.098$	$\bar{M} = 0.71$
	$\kappa = 0.006$	$k_2 = 0.803$	$\kappa_s = 0.0076$	$\upsilon = 0.3$

[1] p_{y0} is a soil constant only for compacted soils.

Table 4. Initial state

	$\bar{p} = 50$ kPa	$s = 300$ kPa
	$e = 1.208$	$S_r = 0.601$
	$p^* = 230$ kPa	$s^* = 164$ kPa
SFG model	$p_{yn0} = 141$ kPa	$s_D = 300$ kPa

	--	s_{sa} = 60 kPa
Wheeler et al. (2003) model	$p_0^* = 273$ kPa	$s_D^* = 164$ kPa

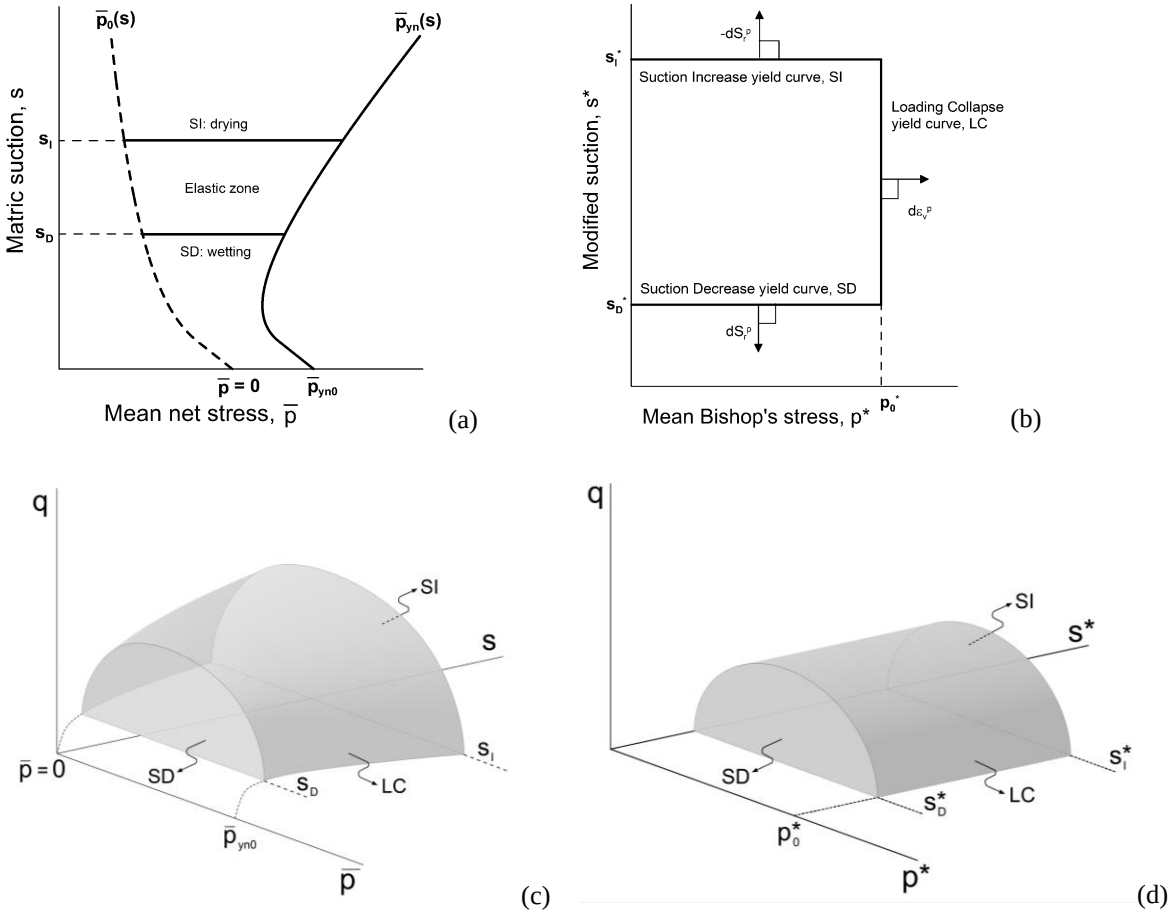

Figure 1. Yield surfaces for isotropic and triaxial stress states: (a) and (c) SFG model for a compacted soil (Sheng et al., 2008a); (b) and (d) Wheeler et al. (2003) model

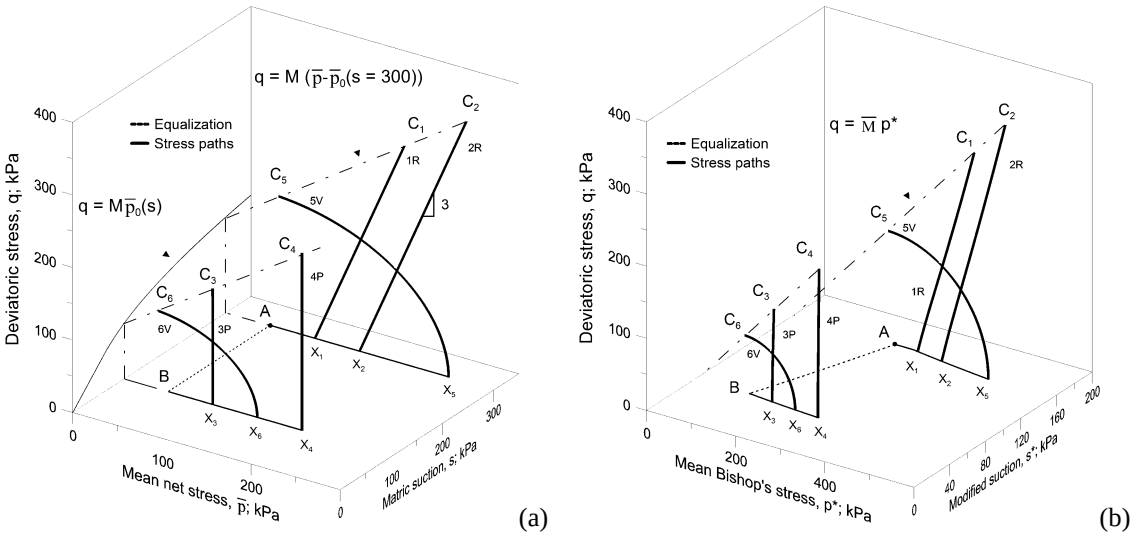

Figure 2. Stress paths: (a) SFG model in the $\bar{p}$:*q*:*s* space; (b) Wheeler et al. (2003) model in the p^*:*q*:s^* space

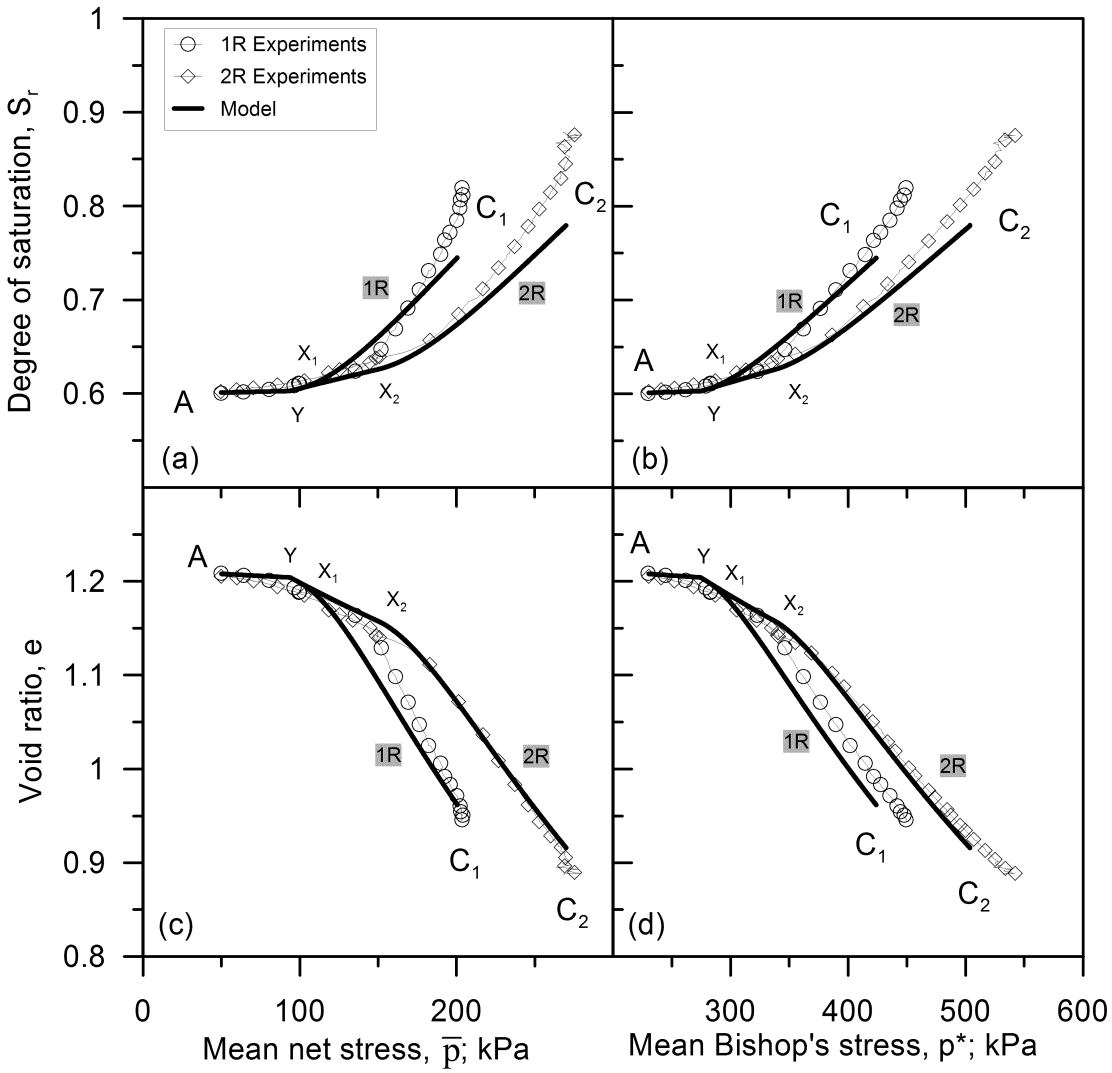

Figure 3. Comparison between SFG model simulations and experimental results for Type R tests at *s* = 300 kPa: (a) degree of saturation against mean net stress; (b) degree of saturation against mean Bishop's stress; (c) void ratio against mean net stress; (d) void ratio against mean Bishop's stress

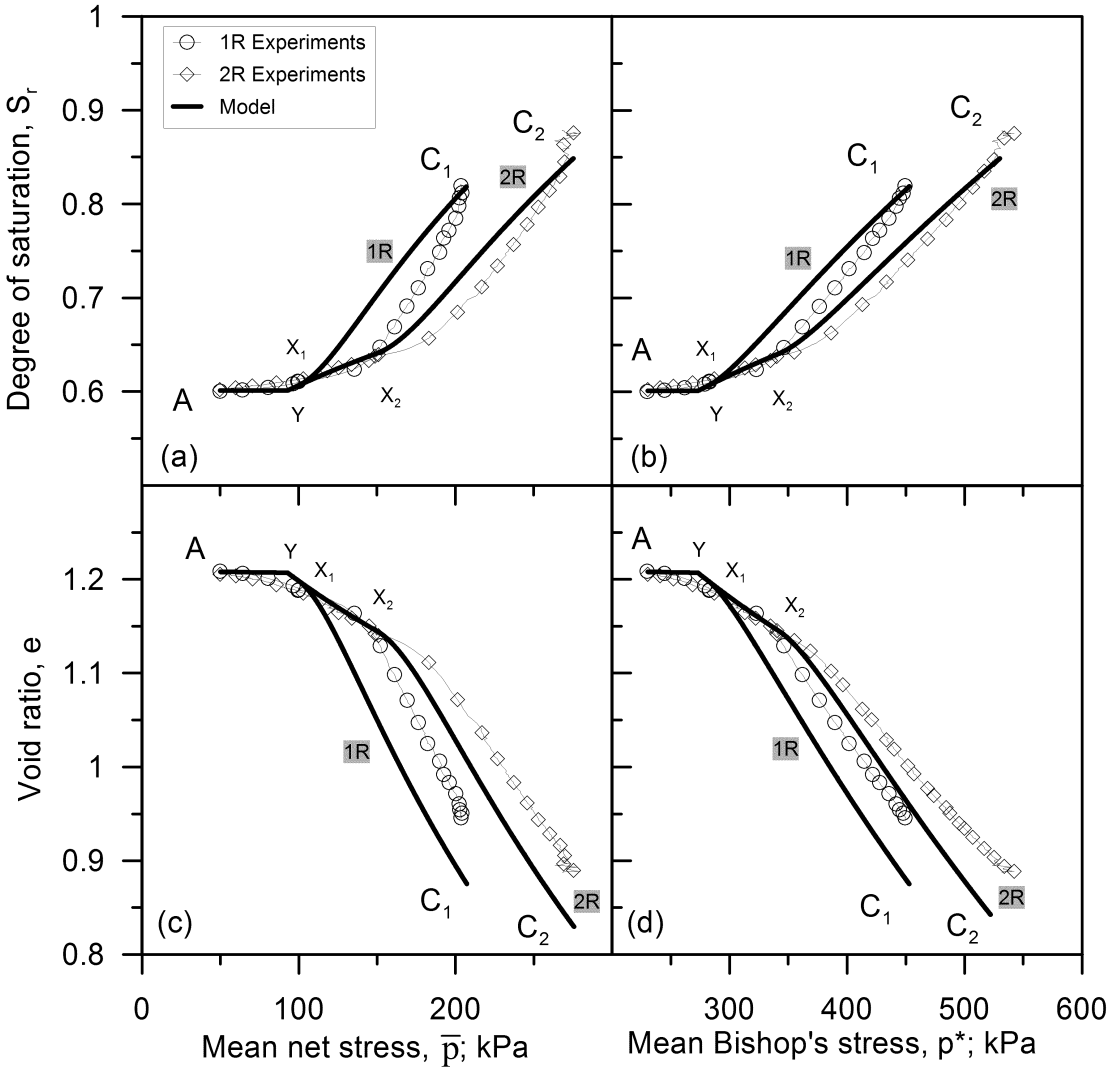

Figure 4. Comparison between Wheeler et al. (2003) model simulations and experimental results for Type R tests at s = 300 kPa: (a) degree of saturation against mean net stress; (b) degree of saturation against mean Bishop's stress; (c) void ratio against mean net stress; (d) void ratio against mean Bishop's stress

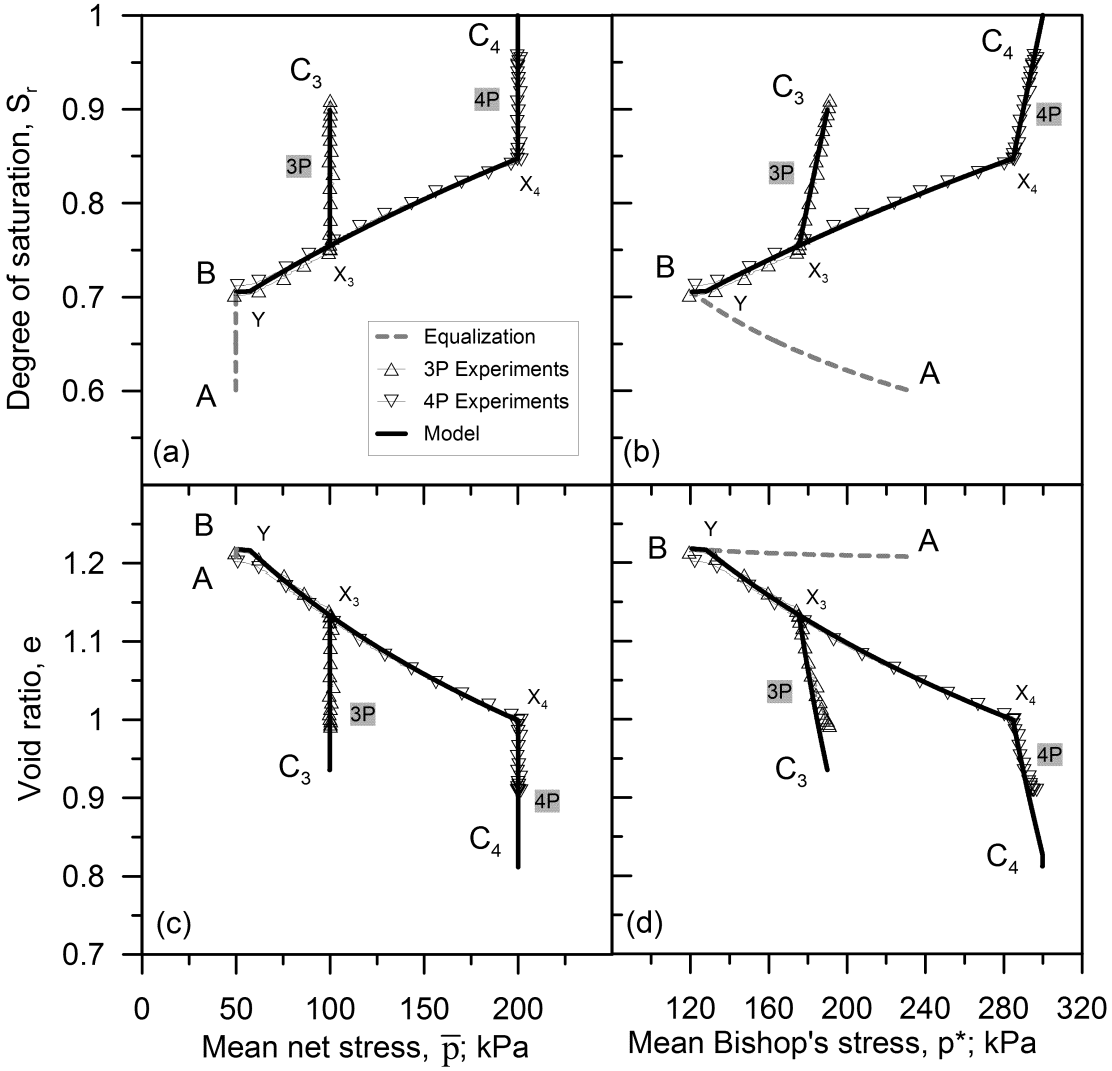

Figure 5. Comparison between SFG model simulations and experimental results for Type P tests at *s* = 100 kPa: (a) degree of saturation against mean net stress; (b) degree of saturation against mean Bishop's stress; (c) void ratio against mean net stress; (d) void ratio against mean Bishop's stress

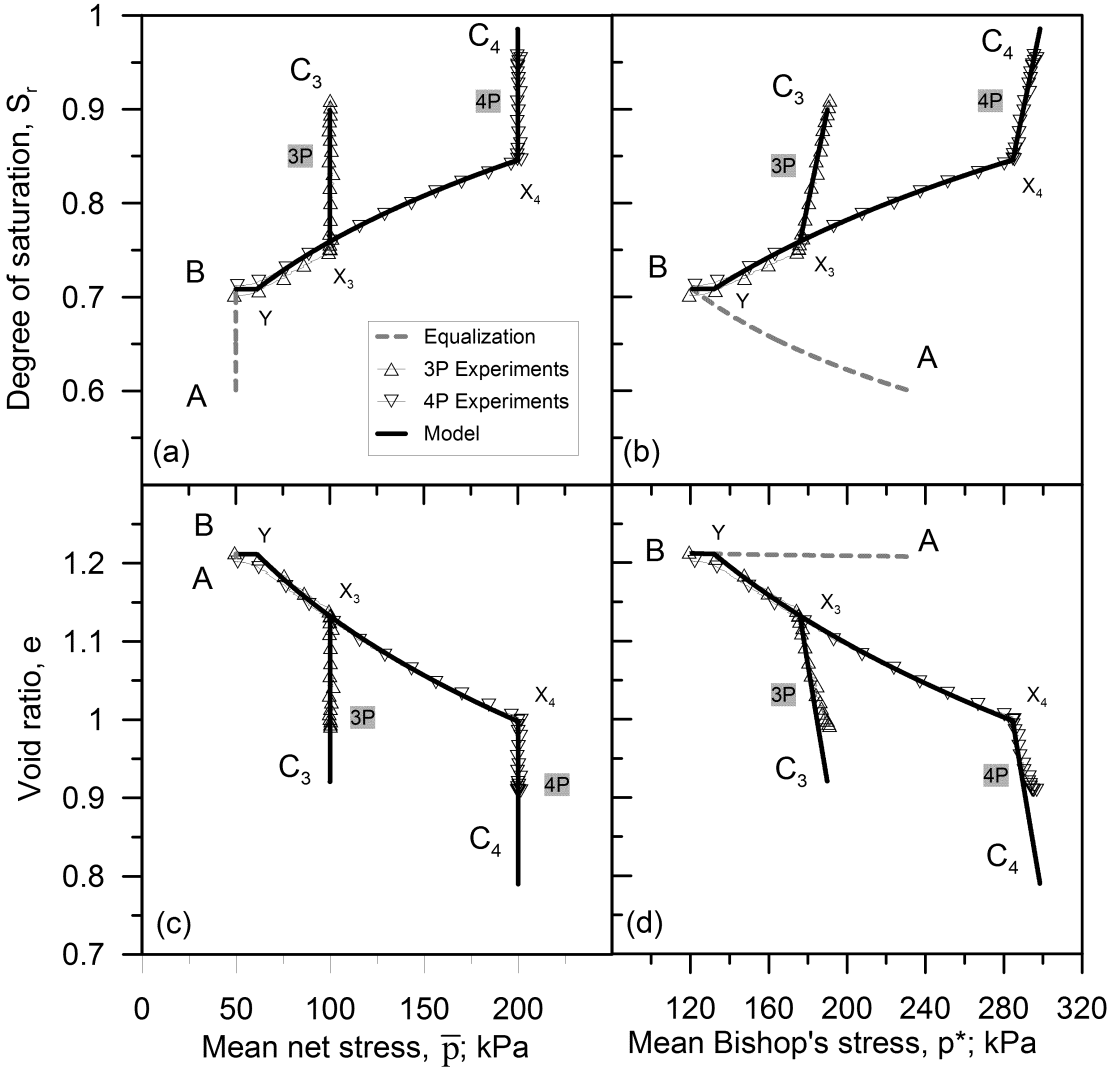

Figure 6. Comparison between Wheeler et al. (2003) model simulations and experimental results for Type P tests at s = 100 kPa: (a) degree of saturation against mean net stress; (b) degree of saturation against mean Bishop's stress; (c) void ratio against mean net stress; (d) void ratio against mean Bishop's stress

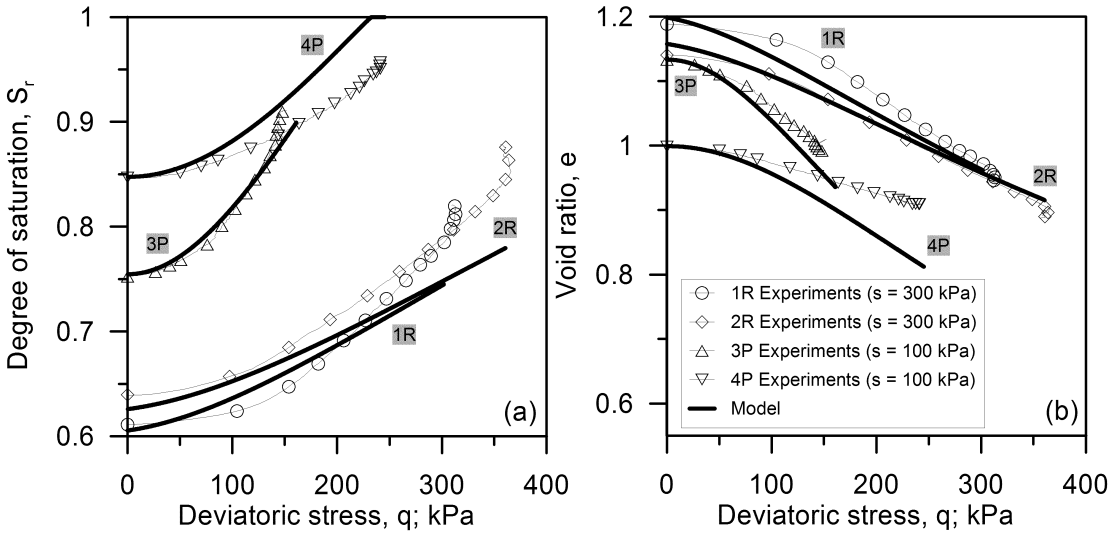

Figure 7. Comparison between SFG model simulations and experimental results for Types R and P tests: (a) degree of saturation against deviator stress; (b) void ratio against deviator stress

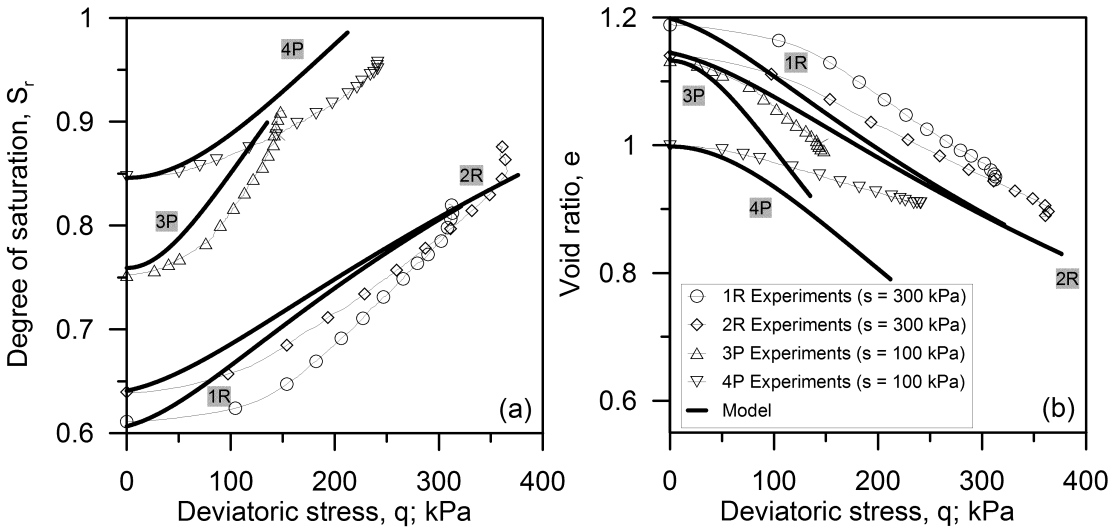

Figure 8. Comparison between Wheeler et al. (2003) model simulations and experimental results for Types R and P tests: (a) degree of saturation against deviator stress; (b) void ratio against deviator stress

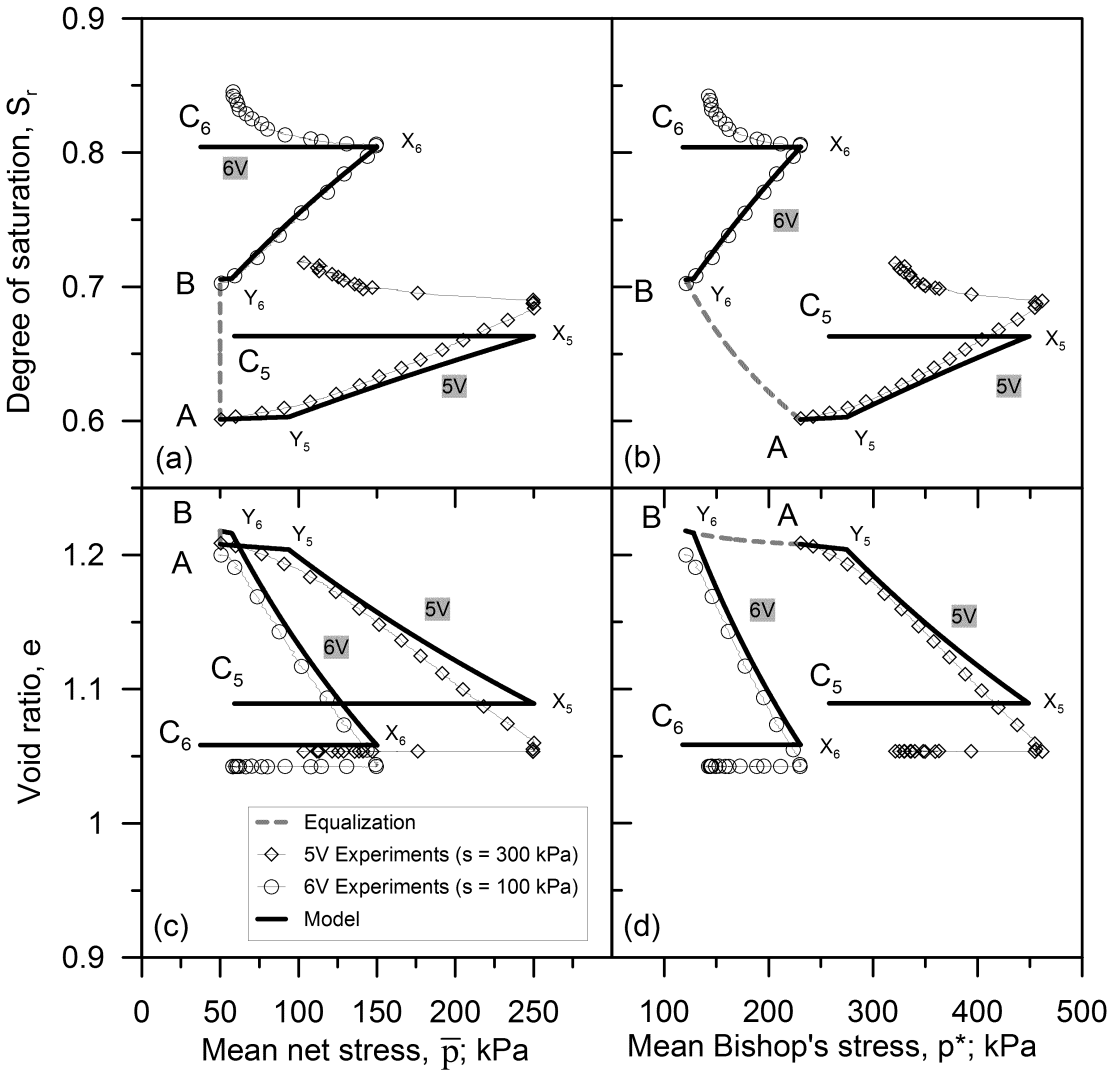

Figure 9. Comparison between SFG model simulations and experimental results for Type V tests: (a) degree of saturation against mean net stress; (b) degree of saturation against mean Bishop's stress; (c) void ratio against mean net stress; (d) void ratio against mean Bishop's stress

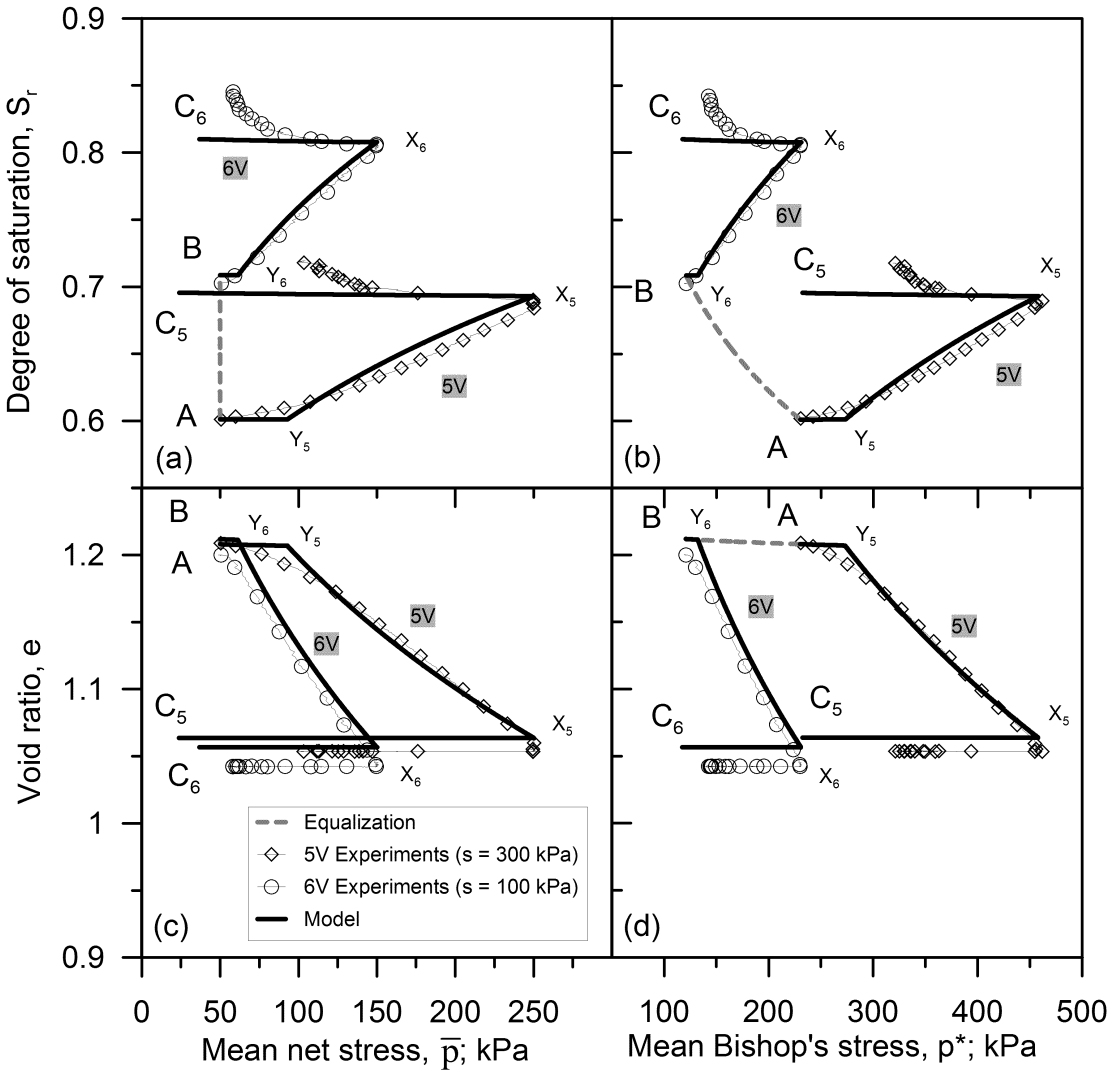

Figure 10. Comparison between Wheeler et al. (2003) model simulations and experimental results for Type V tests: (a) degree of saturation against mean net stress; (b) degree of saturation against mean Bishop's stress; (c) void ratio against mean net stress; (d) void ratio against mean Bishop's stress

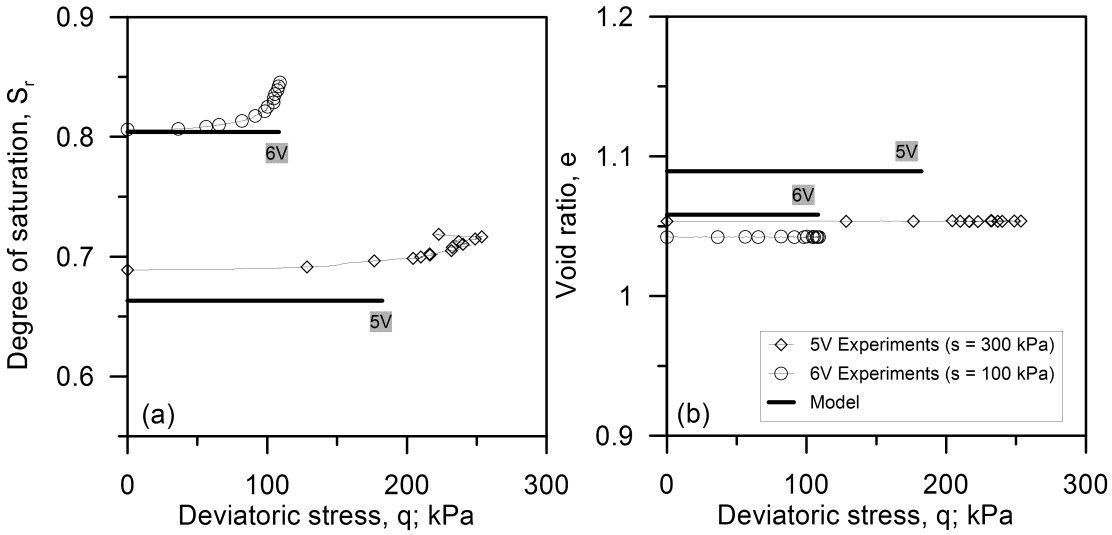

Figure 11. Comparison between SFG model simulations and experimental results for Type V: (a) degree of saturation against deviator stress; (b) void ratio against deviator stress

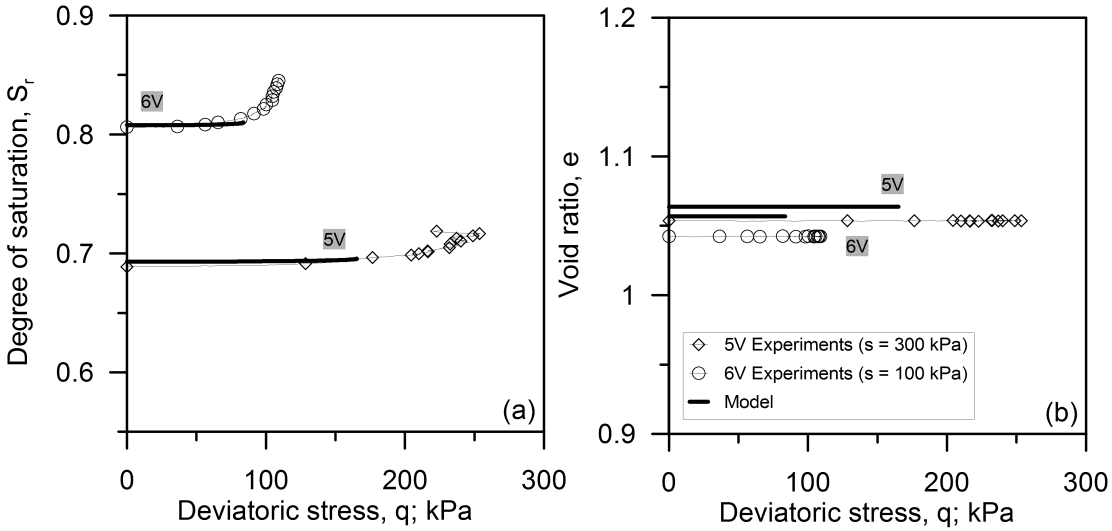

Figure 12. Comparison between Wheeler et al. (2003) model simulations and experimental results for Type V: (a) degree of saturation against deviator stress; (b) void ratio against deviator stress

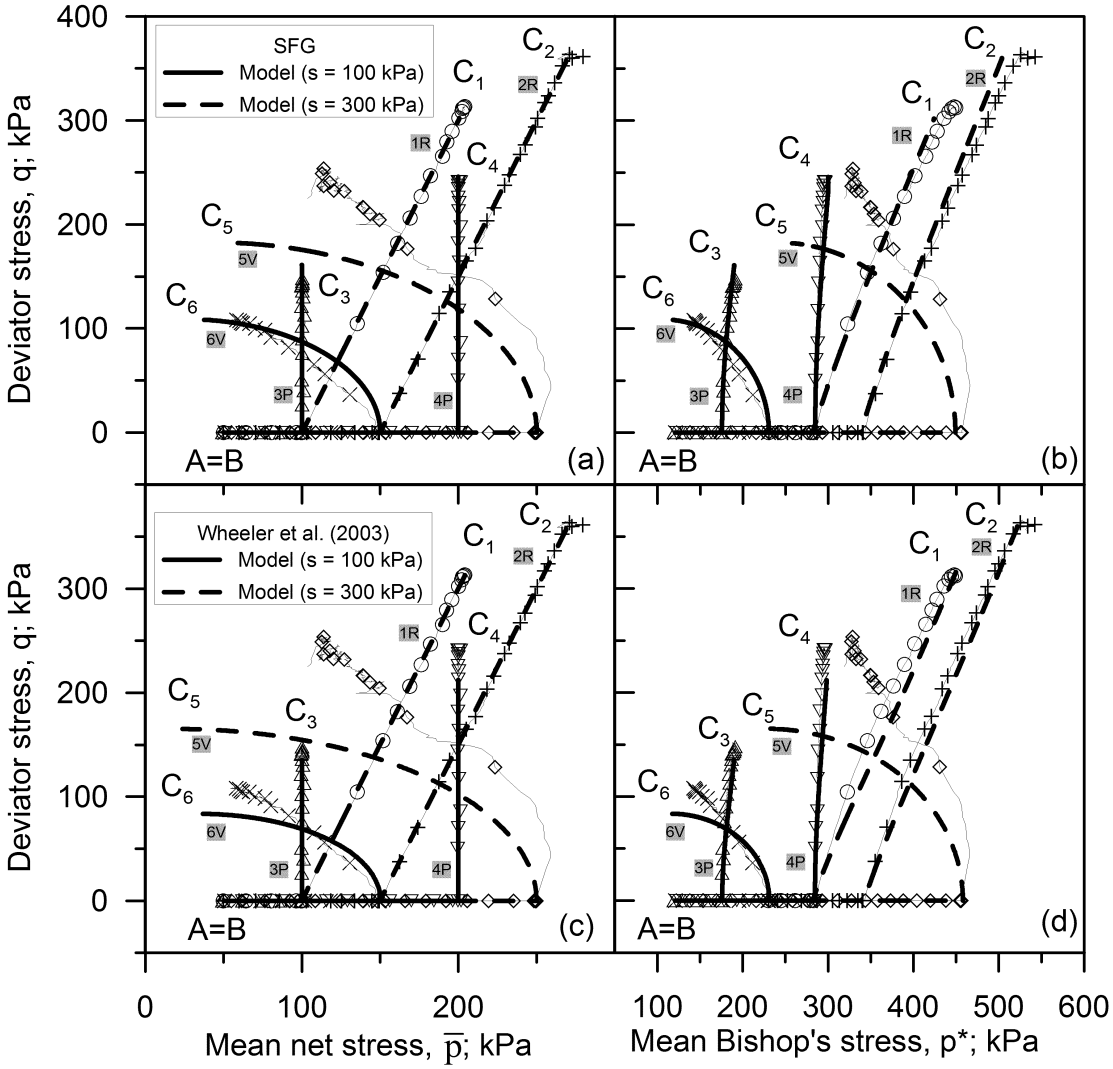

Figure 13. Comparison between experimental results and model simulations: (a) and (b) SFG model (Sheng et al., 2008a); (c) and (d) Wheeler et al. (2003) model